Journal of Science: Advanced Materials and Devices 2 (2017) 59–68

Contents lists available at ScienceDirect

Journal of Science: Advanced Materials and Devices

journal homepage: www.elsevier.com/locate/jsamd

Original Article

Luminescence studies on the europium doped strontium metasilicate phosphor prepared by solid state reaction method

Ishwar Prasad Sahu [a, *], D.P. Bisen [a], Raunak Kumar Tamrakar [b], K.V.R. Murthy [c], M. Mohapatra [d]

[a] School of Studies in Physics & Astrophysics, Pt. Ravishankar Shukla University, Raipur, C.G. 492010, India
[b] Department of Applied Physics, Bhilai Institute of Technology, Durg, C.G. 491001, India
[c] Faculty of Technology and Engineering, MS University of Baroda, Baroda, Gujarat 390001, India
[d] Radiochemistry Division, Bhabha Atomic Research Centre, Mumbai, M.H. 400085, India

ARTICLE INFO

Article history:
Received 7 November 2016
Received in revised form
31 December 2016
Accepted 15 January 2017
Available online 31 January 2017

Keywords:
Monoclinic
Color purity
Quantum efficiency
Stress sensor
Piezo-electricity

ABSTRACT

Europium doped strontium meta-silicate (namely $SrSiO_3:Eu^{3+}$) phosphor was prepared by a high temperature solid state reaction method. The sintered $SrSiO_3:Eu^{3+}$ phosphor possesses a monoclinic structure by the XRD. Energy dispersive X-ray spectrum (EDS) confirms the presence of elements in the desired sample. Thermoluminescence (TL) kinetic parameters such as activation energy (E), order of kinetics (b), and frequency factor (s) were calculated by the peak shape method. The orange–red emission was shown to originate from the $^5D_0$–^7F_J (J = 0, 1, 2, 3, 4) transitions of Eu^{3+} ions as the sample was excited at 396 nm. The $SrSiO_3:Eu^{3+}$ phosphor with almost pure orange-red color purity (99.62%) shows the quantum efficiency of 10.2% (excited by 396 nm), which is higher than those of commercial red phosphors $Y_2O_3:Eu^{3+}$ and $Y_2O_2S:Eu^{3+}$ with quantum efficiencies of 9.6% (excited by 394 nm) and 4.2% (excited by 395 nm), respectively. Mechanoluminescence (ML) intensity of the $SrSiO_3:Eu^{3+}$ phosphor was also found to increase linearly with increasing the impact velocity of the moving piston, suggesting that the discussed phosphor can be used as a stress sensor.

1. Introduction

The phosphors are widely used in emissive displays. However, all currently used phosphors still need considerable improvement, such as lower current saturation, higher efficiency, and better chromaticity [1]. Oxide based phosphors (including silicate phosphors) are more chemically and physically stable than sulfide and aluminates phosphors under high Coulomb loading. Metal silicates have been widely reported as promising host materials for rare earth and transition metal ions with excellent luminescence properties in blue, green and red spectral regions [2]. Strontium silicate phosphor would be ideal from the manufacturing point of view, because both strontium and silica are abundant and cheap. These materials are widely used in the illumination, display devices, storage devices, medical instruments and many more [3,4].

Rare earth oxides (RE_2O_3) are the most stable rare earth compounds, in which the rare earth ions hold typically a trivalent state [5]. Rare earth oxides have been widely used in the field of luminescent devices, optical transmission, bio-chemical probes, medical diagnosis and so forth, because of their optical, electronic and chemical properties resulting from their 4f electrons [6,7]. Inorganic compounds doped with trivalent europium cations (Eu^{3+}) are used for many different applications. Luminescence properties of Eu^{3+} ions involve intra $4f^6(4f–4f)$ transitions mechanisms between the excited state to the ground state [8,9]. The emission wavelength of the 4f–4f transition of Eu^{3+} is relatively insensitive to the host and temperature because the 4f shell is shielded by the outer filled 5s and 5p shells. Eu^{3+} ions were employed in luminescent devices such as fluorescent lamps and cathode ray tubes [10]. Currently transitions of Eu^{3+} ions have attracted considerable interest owing to the attempt to develop novel phosphors that can improve the color temperatures and the color rendering index (CRI) of White Light Emitting Diode (WLED) [11].

Recently, white light emitting diodes (WLEDs) are expected to replace conventional incandescent and fluorescent lamps in the

* Corresponding author.
E-mail address: ishwarprasad1986@gmail.com (I.P. Sahu).
Peer review under responsibility of Vietnam National University, Hanoi.

http://dx.doi.org/10.1016/j.jsamd.2017.01.001

near future because of their benefits in terms of high brightness, reliability, long life time, low environmental impact and energy-saving. At present, the common way for manufacturing WLEDs is to combine a blue LED with $Y_3Al_5O_{12}:Ce^{3+}$ phosphor [12]. Although this type of WLEDs has a high luminous efficiency, it still reveals a low CRI because of deficiency in the red light component [13,14]. Thus, it is needed to develop more efficient red or orange–red emitting phosphors suitable for the fabrication of WLEDs. So, we synthesized $SrSiO_3:Eu^{3+}$ phosphors and studied their luminescent properties. To the best of our knowledge the photoluminescence (PL) and mechanoluminescence (ML) properties of Eu^{3+} doped $SrSiO_3$ phosphor prepared by a solid state reaction method has been reported in the literature. Our study shows that the synthesized $SrSiO_3:Eu^{3+}$ phosphor possesses a higher luminous efficiency as compared to other commercial phosphors such as $Y_2O_3:Eu^{3+}$ and $Y_2O_2S:Eu^{3+}$.

2. Experimental

2.1. Phosphor synthesis

Europium doped strontium meta-silicate phosphor was prepared by the conventional high temperature solid state reaction method. The starting materials were strontium carbonate [$SrCO_3$ (99.90%)], silicon di-oxide [SiO_2 (99.99%)] and europium oxide [Eu_2O_3 (99.99%)], with all of analytical grade (A.R.); employed in this experiment. The contributions of europium oxide in the $SrSiO_3:Eu^{3+}$ phosphor was 2.0 mol%. Boric acid [H_3BO_3(99.99%)] was added as flux. The chemical reaction used for stoichiometry calculation is:

$$SrCO_3 + SiO_2 \xrightarrow{1250^{\circ}C} SrSiO_3 + CO_2\uparrow$$

$$2SrCO_3 + 2SiO_2 + 2Eu_2O_3 \xrightarrow{1250^{\circ}C} 2SrSiO_3 : Eu^{3+} + 2CO_2 + 3O_2\uparrow \quad (1)$$

Initially, raw materials were weighed according to the nominal compositions of $SrSiO_3:Eu^{3+}$ phosphor. Then the powders were mixed and milled thoroughly for 2 h using mortar and pestle. The ground sample was placed in an alumina crucible and subsequently fired at 1250 °C for 3 h in an air. At last the nominal compounds were obtained after the cooling down of a programmable furnace and the final products were grounded into powder for structural and optical characterizations.

2.2. Measurement techniques

The powder XRD pattern has been obtained from the Bruker D8 advanced X-ray powder diffractometer and the data were collected over the 2θ range 10°–80°. The morphological image of prepared phosphor was collected by the Field Emission Scanning Electron Microscopy (FESEM). Prepared phosphor was coated with a thin layer of gold (Au) and then the surface morphology of sintered phosphor was observed by FESEM; ZIESS Ulta Plus-55 operated at the acceleration voltage of 15 kV. An Energy dispersive X-ray Spectroscopy (EDS) spectrum was used for the elemental (qualitative and quantitative) analysis of the prepared phosphor. A Fourier Transform Infrared Spectroscopy (FTIR) spectrum was recorded with the help of IR Prestige-21 by SHIMADZU for investigating the finger print and functional groups region of the prepared phosphor. FTIR spectrum was collected in the middle infrared region by mixing the potassium bromide (KBr, IRgrade) with prepared $SrSiO_3:Eu^{3+}$ phosphor. TL glow curve was recorded with the help of TLD reader 1009I by Nucleonix (Hyderabad, India Pvt. Ltd.). Excitation and emission spectrum was recorded on a Shimadzu (RF 5301-PC) spectrofluorophotometer using the Xenon lamp (150 W) as the excitation source. The color chromaticity coordinates were obtained according to CIE 1931. The decay curve was obtained using a time resolved fluorescence spectroscopy (TRFS) from Horiba Jobin Yvon IBH to measure the fluorescence lifetimes of the prepared phosphor (pulsed lasers as excitation source). ML measurement was observed by the homemade lab system comprising of an RCA-931A photomultiplier tube (PMT) and ML glow curve can be plotted with the help of SM-340 application software installed in a computer attached with the storage oscilloscope. TL and ML spectrum was recorded with the help of different band pass interference (400–700 nm) filters. All measurements were carried out in the room temperature.

3. Results and discussion

3.1. XRD analysis

The typical XRD patterns of $SrSiO_3$ and $SrSiO_3:Eu^{3+}$ phosphors with JCPDS file are shown in Fig. 1a. These XRD patterns were consistent with JCPDS 24-1230 file [15]. In Fig. 1b, the position and intensity of diffraction peaks of prepared $SrSiO_3:Eu^{3+}$ phosphor were matched and found to be consistent with the standard Crystallography Open Database (COD) card No. 96-200-6167 by MATCH 2 software. The figure of merit (FOM) while matching these was 0.8446 (85%), indicating that the phase of the prepared phosphor agrees with the standard pattern COD card No. 96-200-6167. From the analysis of $SrSiO_3$ and $SrSiO_3:Eu^{3+}$ XRD patterns, it was found that the little amount of doped Eu^{3+} ions has no effect on the $SrSiO_3$ phase structure. From Fig. 1b, it can be concluded that the prepared samples were chemically and structurally strontium meta-silicate ($SrSiO_3$) phosphors.

The indexing and refinement of lattice parameters were investigated using software Celref V3. The results indicate that the $SiO_3:Eu^{3+}$ phosphor exhibits a monoclinic structure with space group C12/c1. The lattice parameters of monoclinic $SrSiO_3:Eu^{3+}$ phosphor was determined to be a = 12.327 Å, b = 7.138 Å, c = 10.881 Å, $\alpha = 90^{\circ}$, $\beta = 111.57^{\circ}$, $\gamma = 90^{\circ}$ and cell volume = 892.06 (Å)^3, Z = 12 is nearly same [a = 12.333 Å, b = 7.146 Å, c = 10.885 Å, $\alpha = 90^{\circ}$, $\beta = 111.57^{\circ}$, $\gamma = 90^{\circ}$ and cell volume = 892.13 (Å)^3, Z = 12 signifying the proper preparation of the discussing $SrSiO_3:Eu^{3+}$ phosphor. There are few extra peaks in an observed XRD pattern which could be due to the number of stacking faults induced by the presence of doping ions and also due to secondary phases and impurities formed during the elaboration process. The calculated spectrum confirmed the presence of the monoclinic $SrSiO_3:Eu^{3+}$ phosphor.

3.2. Field Emission Scanning Electron Microscopy (FESEM)

FESEM study was carried out to obtain information about surface morphology, grain size, and shape of the synthesized phosphor. The morphologies of the prepared $SrSiO_3:Eu^{3+}$ phosphor were also observed by means of FESEM in Fig. 2. From the FESEM image, it can be observed that the prepared phosphor consists of particles with different size distribution. The morphological images of the prepared $SrSiO_3:Eu^{3+}$ phosphor shows that particles were aggregated tightly due to the high temperature synthesis process.

3.3. Fourier Transform Infrared (FTIR) spectra

FTIR spectra have been widely used for the identification of organic and inorganic compounds. Fig. 3 shows the FTIR spectra of $SrSiO_3:Eu^{3+}$ phosphor. The appearance of the band related to the stretching vibrations of OH groups (~3439.43 cm^{-1}) in the IR

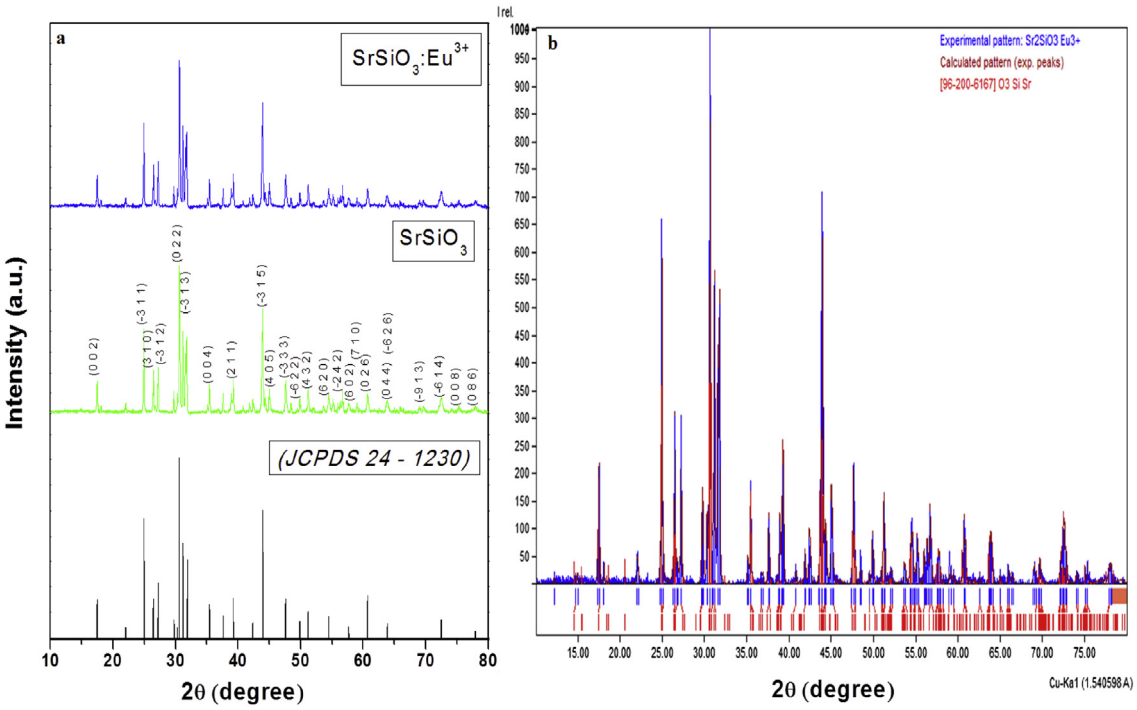

Fig. 1. (a) XRD patterns of $SrSiO_3$ and $SrSiO_3$:Eu^{3+} phosphors with the JCPDS file (b) Observed, calculated and standard XRD patterns of $SrSiO_3$:Eu^{3+} phosphor.

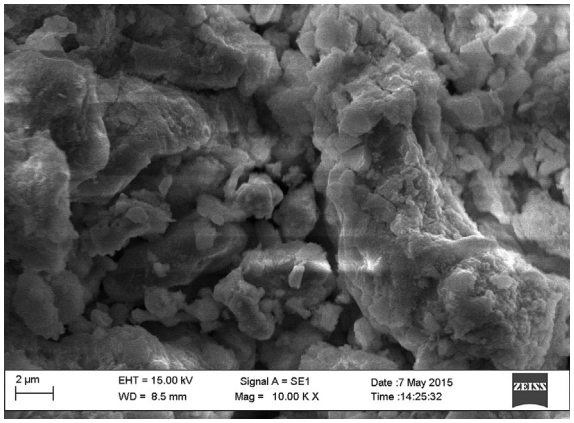

Fig. 2. FESEM micrograph of $SrSiO_3$:Eu^{3+} phosphor.

spectrum, was the evidence of hydration resulting from the absorption of atmospheric moisture. The asymmetric stretching of (CO_3^{2-}) carbonates can be observed ~ 2729.54, 1979.38 cm^{-1}. These bands are due to slight carbonation of the raw materials [$SrCO_3$]. The vibration bending of the sharp peaks in the region of ~1427.77 cm^{-1} is assigned due to the Sr^{2+} [16,17].

According to the crystal structure of $SrSiO_3$, the coordination number of strontium can be 8 and 6. Therefore, Sr^{2+} can occupy two alternative lattice sites, eight coordinated site [SrO_8 (Sr_1 site)] and six coordinated site [SrO_6 (Sr_2 site)], and other independent cation sites, namely Si^{4+} [SiO_4] also existed in the crystal lattice. The Si^{4+} cations occupy the tetrahedral sites [18,19]. Eu^{3+} ions can occupy two alternative lattice sites and the coordination number of europium can be 8 and 6 [EuO_8 (Eu_1) and EuO_6 (Eu_2)]. It's hard for Eu^{3+} ions to incorporate the tetrahedral [SiO_4] symmetry, but they can easily incorporate the octahedral [SrO_8] or the hexahedral [SrO_6]. Another fact that supports that the radius of Eu^{3+} (1.07 Å) is very close to that of Sr^{2+} (about 1.12 Å) while being larger than that of Si^{4+} (0.41 Å). Therefore, Eu^{3+} ions are expected to occupy Sr^{2+} sites in the $SrSiO_3$:Eu^{3+} phosphor [20].

In the presented spectrum, the absorption bands of silicate groups are clearly evident. According to previous studies on silicate materials, the position of the bands in ~1100–800 cm^{-1} region can provide information about the number of bridging oxygen atoms, bonded to the silicon atoms. The intense bands of ~1065.55, 981.47, 867.89 and 716.72 cm^{-1} were assigned to the Si–O–Si asymmetric stretch and Si–O symmetric stretch. The bands of ~671.77, 625.86, 543.15 and 490.73 cm^{-1} were due to the Si–O–Si vibrational mode. The groups [SiO_4] constituting ortho-silicates, were the main structural elements, as presented in the discussed FTIR spectra of the $SrSiO_3$:Eu^{3+} phosphor [21,22].

3.4. Thermoluminescence (TL)

In order to study the trap states of the prepared $SrSiO_3$:Eu^{3+} phosphor, TL glow curves were recorded and are displayed in Fig. 4. The phosphor was first irradiated for 10 min using a 365 nm UV source, then the radiation source was removed and the irradiated sample was heated at a linear heating rate of 5 °C/s, from room temperature to 300 °C. Initially the TL intensity increases with temperature, attains a peak value for a particular temperature, and then decreases with further increase in temperature. A single glow peak of $SrSiO_3$:Eu^{3+} phosphor was obtained at 166.79 °C, therefore high energy was required to release the trapped electrons; hence long storage of trapped charge carriers at normal working temperature was achieved and thus the thermal stability was ensured. The single isolated peak due to the formation of only one type of luminescence center which was created due to the UV irradiation. It is suggested that the recombination center associated with the glow peak at the temperature interval arises from the presence of liberated pairs probably due to the thermal release of electron/holes from electron/hole trap level and

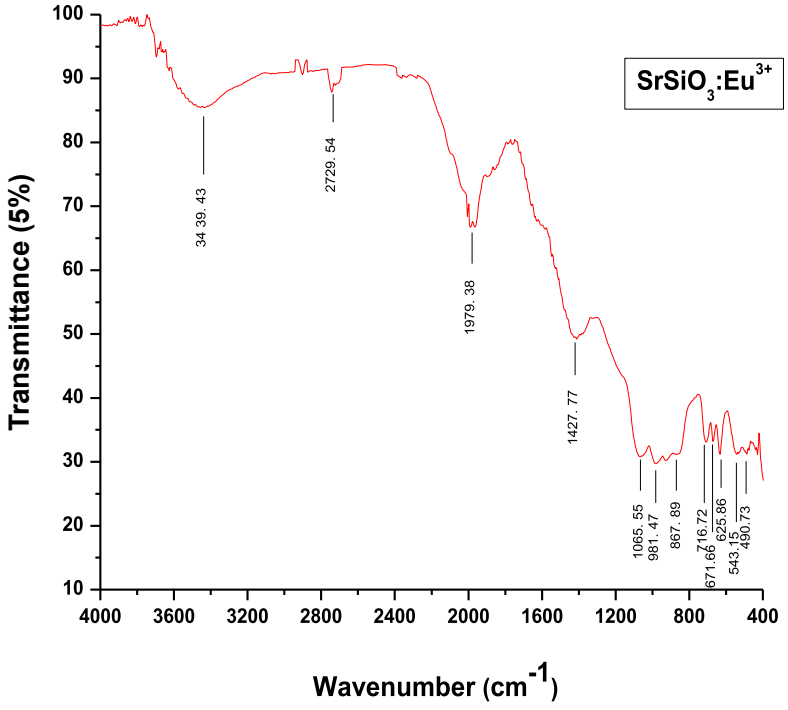

Fig. 3. FTIR Spectra of $SrSiO_3:Eu^{3+}$ phosphor.

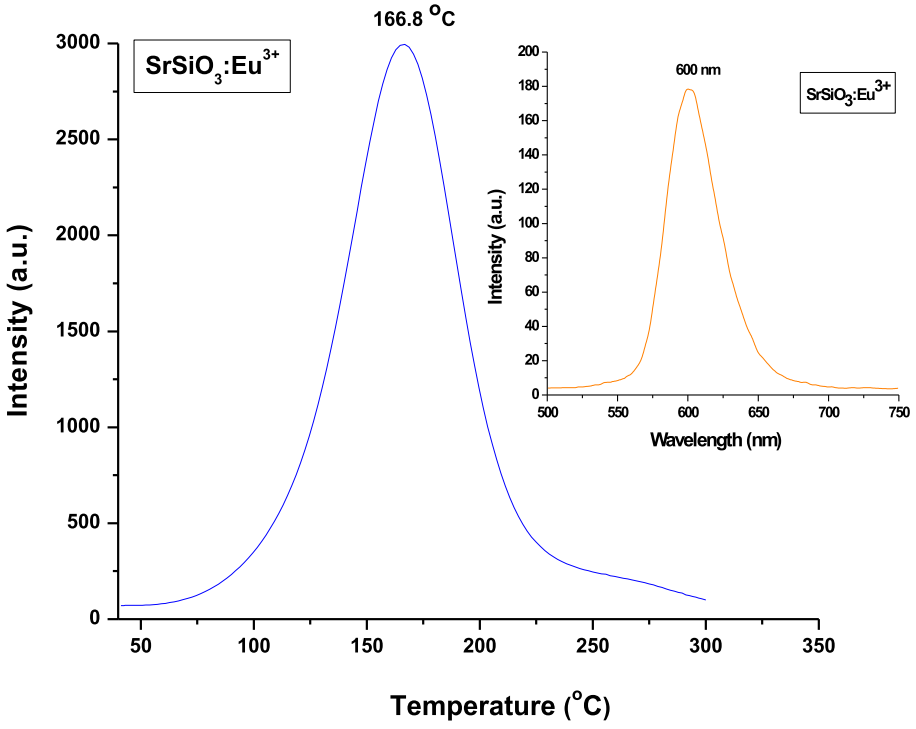

Fig. 4. TL glow curve of $SrSiO_3:Eu^{3+}$ phosphor for a 10 min UV irradiation [Inset – TL spectra of $SrSiO_3:Eu^{3+}$ phosphor].

their recombination at the color centers. It is also known that the doping of the rare earth ions increases the lattice defects which have existed already in the host. The TL kinetic parameters were calculated and listed in Table 1.

Fig. 4 (inset) shows the TL emission spectra of $SrSiO_3:Eu^{3+}$ phosphor. TL emission spectra of $SrSiO_3:Eu^{3+}$ phosphor shows a broad peak around 600 nm corresponds to orange–red color in the visible region. The TL emission spectrum of $SrSiO_3:Eu^{3+}$ phosphor confirm the single isolated peak due to the formation of only one type of luminescence centers created due to the UV irradiation.

3.4.1. *Determination of kinetic parameters*

There are various methods for evaluating the trapping parameters from TL glow curves. For example, when one of the TL glow

Table 1
Activation energy (E), frequency factor (s^{-1}) and shape factor (μ_g) for UV irradiated $SrSiO_3:Eu^{3+}$ phosphor.

UV min	HTR	T_1 (°C)	T_m (°C)	T_2 (°C)	τ (°C)	δ (°C)	ω (°C)	$\mu_g = \delta/\omega$	Activation energy (eV)	Frequency factor
10	5	136.1	166.8	193.82	30.69	27.03	57.72	0.47	0.94	2.26×10^{10}

peaks is highly isolated from the others, the experimental method such as peak shape method is appropriate to determine kinetic parameters [23]. The TL parameters for the prominent glow peaks of the prepared phosphor were calculated using the peak shape method [24,25]. The relationship between the frequency factor's' and the activation energy 'E' is given by the Equation (2)

$$\frac{\beta E}{kT_m^2} = s\left[1 + (b-1)\frac{2kT_m}{E}\right]\exp(E/KT_m) \quad (2)$$

where, k is Boltzmann constant, E is activation energy, b is order of kinetics, T_m is temperature of peak position, and β is the heating rate. In the present work $\beta = 5$ °C/s. Trap depth for second order kinetics is calculated using the Equation (3)

$$E = 2kT_m\left(1.76\frac{T_m}{\omega} - 1\right) \quad (3)$$

where ω is the total half width intensity $\omega = \tau + \delta$, τ is the half width at the low temperature side of the peak ($\tau = T_m - T_1$); δ is the half width towards the fall-off side of the glow peak ($\delta = T_2 - T_m$), and T_m is the peak temperature at the maximum. The shape factor $\mu_g = \delta/\omega$. The shape factor (μ_g) is to differentiate between first and second order TL glow peak. (μ_g) = 0.39–0.42 for the first order kinetics and (μ_g) = 0.49–0.52 for the second order kinetics and (μ_g) = 0.43–0.48 for the intermediate (mixed) order of kinetics [26–28].

The calculated kinetic parameters of $SrSiO_3:Eu^{3+}$ phosphor by the peak shape method are given in Table 1. In our case, the value of shape factor (μ_g) has been calculated to be 0.47, which indicates that it is a case of mixed (intermediate) order kinetics, approaching towards second order [29]. The activation energy for the prepared $SrSiO_3:Eu^{3+}$ phosphor was estimated to be 0.94 eV.

3.5. Photoluminescence (PL)

The emission spectrum of $SrSiO_3:Eu^{3+}$ phosphor excited at 396 nm is shown in Fig. 5. It can be seen that the spectrum was composed of several sharp lines from the characteristic Eu^{3+} emission. It exhibits a broad band in the UV region centered at about 240 nm, and several sharp lines between 300 and 400 nm Eu^{3+} ions have a $4f^6$ configuration, which needs to gain one more electron to achieve the half-filled $4f^7$ configuration, that is relatively stable compared to partially filled configurations. When Eu^{3+} is linked to the oxygen (O) ligand, there is a chance of electron transfer from O to Eu^{3+} to form Eu^{2+}–O^2 (simply Eu–O). During this, there is a broad absorption band at 230–270 nm, depending on the host. This is known as the Eu–O charge transfer band (CTB). It can be seen from Fig. 5, the excitation spectrum was composed to two major parts: (1) the broad band between 220 and 300 nm, the broad absorption band is a called charge transfer state (CTS) band due to the europium–oxygen interactions, which is caused by an electron transfer from an oxygen 2p orbital to an empty 4f shell of europium and the strongest excitation peak at about 240 nm. (2) A series of sharp lines between 300 and 400 nm, ascribed to the f–f transition of Eu^{3+} ions. The sharp peak is located at 396 nm corresponding to $^7F_0 \rightarrow {}^5L_6$ transition of Eu^{3+} ions. Other weak excitation peaks are located at 320, 330, 346, 363 and 384 nm, which are related to the intra-configurational 4f–4f transitions of Eu^{3+} ions in the host lattices. The prepared $SrSiO_3:Eu^{3+}$ phosphor can be excited by near UV (NUV) at about 396 nm effectively. So, it can match well with UV and NUV-LED, showing a great potential for practical applications [30].

The emission spectrum of $SrSiO_3:Eu^{3+}$ phosphor is shown in Fig. 5 in the range of 400–700 nm. Under the 396 nm excitation, the emission spectrum of our prepared samples was composed of a series of sharp emission lines, corresponding to transitions from the excited states $^5D_0$ to the ground state $^7F_{j\ (j\ =\ 0,1,2,3)}$. The orange emission at about 594 nm belongs to the magnetic dipole $^5D_0 \rightarrow {}^7F_1$ transition of Eu^{3+}, and the transition hardly varies with the crystal field strength. The red emission at 614 nm is ascribed to the electric dipole $^5D_0 \rightarrow {}^7F_2$ transition of Eu^{3+} ions, which is very sensitive to the local environment around the Eu^{3+}, and depends on the symmetry of the crystal field. It is found that the 594 and 614 nm emissions are the two strongest peaks, indicating that there are two Sr^{2+} sites in the $SrSiO_3:Eu^{3+}$ lattice [31]. One site, Sr (I), is inversion symmetry and the other site, Sr (II), is non-inversion symmetry. When doped in $SrSiO_3:Eu^{3+}$ ions occupied the two different sites of Sr (I) and Sr (II). Other two emission peaks located at 580 and 652 nm are relatively weak, corresponding to the $^5D_0 \rightarrow {}^7F_0$ and $^5D_0 \rightarrow {}^7F_3$ typical transitions of Eu^{3+} ions respectively. The strongest emission is associated with the Eu^{3+} electric-dipole transition of $^5D_0 \rightarrow {}^7F_1$, which implies that the Eu^{3+} occupies a center of inversion asymmetry in the host lattice. For the $SrSiO_3:Eu^{3+}$ prepared in our experiment, the strongest orange emission peak is located at 594 nm is dominant. It can be presumed that Eu^{3+} ions mainly occupy with an inversion symmetric center in the host lattice [32].

3.6. CIE chromaticity coordinate

The luminescence color of the sample excited under 396 nm has been characterized by the CIE 1931 chromaticity diagram [33]. The emission spectrum of the $SrSiO_3:Eu^{3+}$ phosphor was converted to the CIE 1931 chromaticity using the photo luminescent data and the interactive CIE software (CIE coordinates calculator) diagram as shown in Fig. 6.

Every natural color can be identified by (x, y) coordinates that are disposed inside the 'chromatic shoe' representing the saturated colors. Luminescence colors of $SrSiO_3:Eu^{3+}$ phosphor are placed in the orange–red (x = 0.564, y = 0.415) corners. The chromatic coordinates of the luminescence of this phosphor are measured and reached to orange–red luminescence. Thus, the $SrSiO_3:Eu^{3+}$ phosphor can be applied to n-UV-based W-LEDs.

The chromaticity diagram of the CIE indicates the coordinates are highly useful in determining the exact emission color and color purity of a sample. Because the color purity is considered as one of the important factors for evaluating the performance of phosphors, the color purity of samples has been calculated by the following Equation (4) [34,35]:

$$\text{Color purity} = \frac{\sqrt{(x-x_i)^2 + (y-y_i)^2}}{\sqrt{(x_d-x_i)^2 + (y_d-y_i)^2}} \cdot 100\%, \quad (4)$$

where (x, y) and (x_i, y_i) are the color coordinates of the light source and the CIE equal-energy illuminant respectively; (x_d, y_d) is the chromaticity coordinate corresponding to the dominant wavelength of light source. For $SrSiO_3:Eu^{3+}$ phosphor, and the

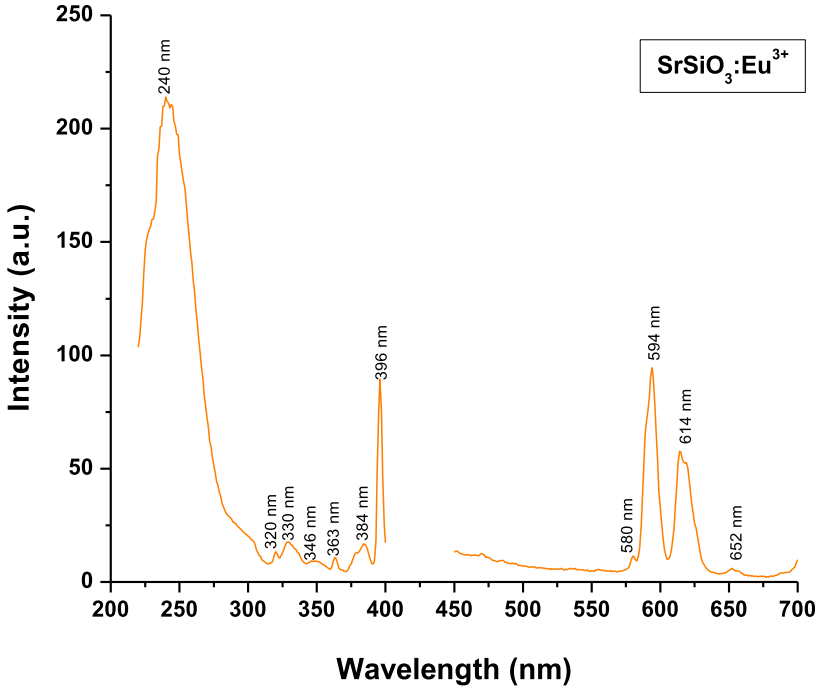

Fig. 5. Excitation and emission spectra of $SrSiO_3:Eu^{3+}$ phosphor.

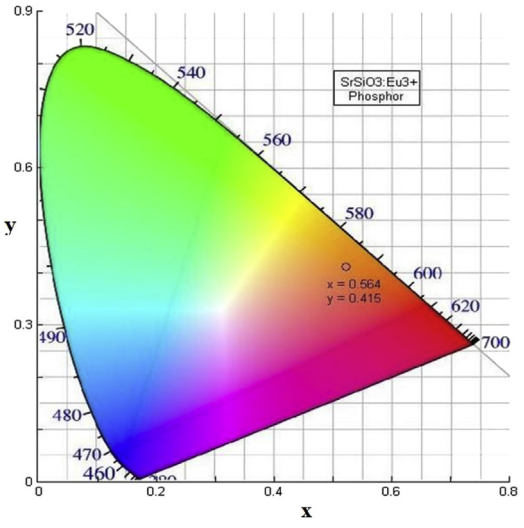

Fig. 6. CIE chromaticity diagram of $SrSiO_3:Eu^{3+}$ phosphor.

coordinates of (x, y) are (0.564, 0.415); the coordinates of (x_i, y_i) are (0.333, 0.333); (x_d, y_d) is (0.565, 0.415); corresponding to the dominant wavelength of 594 nm. Based on these coordinate values and Equation (4), we finally get the color purity of $SrSiO_3:Eu^{3+}$ phosphor as 99.62%. It is worthwhile to mention that the CIE chromaticity coordinates of $SrSiO_3:Eu^{3+}$ phosphor are very close to those corresponding dominant wavelength points, and that almost pure orange-red color purity phosphors have been obtained in our work.

Moreover, since the quantum efficiency of the phosphor is a very important factor in evaluating its potential for the LED application. The luminescence intensity of the discussed $SrSiO_3:Eu^{3+}$ phosphor was also investigated by the absolute quantum efficiencies. Table 2 shows the calculated Quantum Efficiency (QE) of $SrSiO_3:Eu^{3+}$ and $Ba_{4.93}(BO_3)_2(B_2O_5):0.07Sm^{3+}$, $Y_2O_3:Eu^{3+}$, $Y_2O_2S:Eu^{3+}$ commercial red phosphors. It can be seen that $SrSiO_3:Eu^{3+}$ presents the best quantum efficiency of 10.2% (excited by 396 nm). The results demonstrate that $Ba_{4.93}(BO_3)_2(B_2O_5):0.07Sm^{3+}$ are higher than those commercial red phosphors under the near ultraviolet light excitation [36,37]. However, the QEs of $SrSiO_3:Eu^{3+}$ are lower than the red-emitting nitride compound $Sr_2Si_5N_8:Eu^{2+}$ excited by blue (450 nm) light as reported. All the results show that the $SrSiO_3:Eu^{3+}$ orange–red phosphors may be a potential orange–red emitting phosphor excited by near ultraviolet light for white LEDs [38,39].

3.7. Decay

Fig. 7 shows the typical decay curves of $SrSiO_3:Eu^{3+}$ phosphor. The initial afterglow intensity of the sample was high. The decay times of phosphor can be calculated by a curve fitting technique, and the decay curves fitted by the sum of two exponential components have different decay times via Equation (5):

$$I = A_1 \exp(-t/\tau_1) + A_2 \exp(-t/\tau_2) \quad (5)$$

where, I is phosphorescence intensity, A_1, A_2 are constants, t is time, τ_1 and τ_2 are decay times (in microseconds) for the exponential components. Decay curves are successfully fitted by the Equation (5) [40] and the fitting curve results are shown in the inset of Fig. 7 with the standard error. The results indicated that the, decay curves are composed of two regimes, i.e., the initial rapid decaying process and the subsequent slow decaying process.

As it was reported, when Eu^{3+} ions were doped into $SrSiO_3$, they would substitute the Sr^{2+} ions. To keep electro-neutrality of the compound, two Eu^{3+} ions would substitute three Sr^{2+} ions. The process can be expressed as

$$2Eu^{3+} + 3Sr^{2+} \rightarrow 2\,[Eu_{Sr}]^{*} + [V_{Sr}]''. \quad (6)$$

Table 2
Calculated quantum efficiency of different phosphors.

Sr. No.	Phosphors name	Excitation wavelength (nm)	Quantum efficiency (%)
1	$SrSiO_3:Eu^{3+}$	396	10.2
2	$Ba_{4.93}(BO_3)_2(B_2O_5):0.07Sm^{3+}$	403	11.0
3	$Y_2O_3:Eu^{3+}$	394	9.6
4	$Y_2O_2S:0.05Eu^{3+}$	395	4.2
5	$Sr_2Si_5N_8:Eu^{2+}$	450	75.0%

Each substitution of two Eu^{3+} ions would create two positive defects of $[Eu_{Sr}]^*$ capturing electrons and one negative vacancy of $[V_{Sr}]''$. These defects act as trapping centers for charge carriers. Then the vacancy $[V_{Sr}]''$ would act as a donor of electrons while the two $[Eu_{Sr}]^*$ defects become acceptors of electrons. By thermal stimulation, electrons of the $[V_{Sr}]''$ vacancies would then transfer to the Eu^{3+} sites. The results indicate that the depth of the trap is too shallow leading to a quick escape of charge carriers from the traps resulting in a fast recombination rate in microseconds (μs) [41].

3.8. Mechanoluminecsnce (ML)

ML is the phenomenon of light emission from a solid as a response to a mechanical stimulus given to it [42]. ML can by excited by grinding, cutting, cleaving, rubbing, shaking, scratching, compressing, loading, crushing or impulsive de-formation of solids [43]. In the present study, we deformed the prepared $SrSiO_3:Eu^{3+}$ phosphor by the impulsive deformation technique. During the deformation of a solid, great number of physical processes may occur within very short time intervals, which may excite or stimulate the process of photon emission. It is seen that when moving piston was released at particular height, then ML emission also took place [44,45].

Fig. 8 shows the characteristic glow ML curve (ML intensity versus time) for different heights. When the moving piston was dropped onto the prepared phosphor at different heights, light emits. The photon emission time is nearly 2 ms, when the prepared $SrSiO_3:Eu^{3+}$ phosphor fractures. In these ML measurements, the maximum ML intensity has been obtained for the 50 cm dropping height, and the ML intensity increases with the falling height of the moving piston [46]. Fig. 8 (Inset) shows that the characteristic curve between ML intensity versus impact velocity of $SrSiO_3:Eu^{3+}$ phosphor. The ML intensity increases linearly with increasing the falling height of the moving piston; that is, the ML intensity depends upon the impact velocity of the moving piston. The ML intensity of $SrSiO_3:Eu^{3+}$ phosphor increases linearly with increasing the mechanical stress [47].

The relationship between semi-log plots of ML intensity versus $(t-t_m)$ for $SrSiO_3:Eu^{3+}$ phosphor shown in Fig. 9, and the lines were fitted using the Equation (7)

$$\tau = \frac{1}{slope\ \ of\ \ straight\ \ line} \tag{7}$$

The fitting results show that the decay constant (τ) varies from 0.77 to 0.90 ms. The ML decay constant value is increased with the impact velocity, and reaches a maximum for the maximum impact velocity (Table 3).

Fig. 10 shows the ML spectrum of$SrSiO_3:Eu^{3+}$ phosphor. The Eu^{3+} ion with the $4f^6$ electron configuration shows efficient luminescence resulting from the 4f–4f transition and was an important activator for various kinds of practical phosphor [48]. From Fig. 10, it can be observed that the ML spectrum at 600 nm (orange–red region), is similar to the PL (594 nm) and TL spectrum (600 nm) of $SrSiO_3:Eu^{3+}$ phosphor. This implies that ML was emitted from the same emitting center of Eu^{3+} ions as PL and TL, which is produced by the transition of Eu^{3+} ions, corresponding to transitions from the excited states $^5D_0$ to the ground state ^7F_j $(j = 1, 2)$ [49].

When mechanical stress, such as compress, friction and striking, and so on, were applied onto the sintered $SrSiO_3:Eu^{3+}$ phosphor, piezoelectric field can be produced. Therefore, in such phosphor the

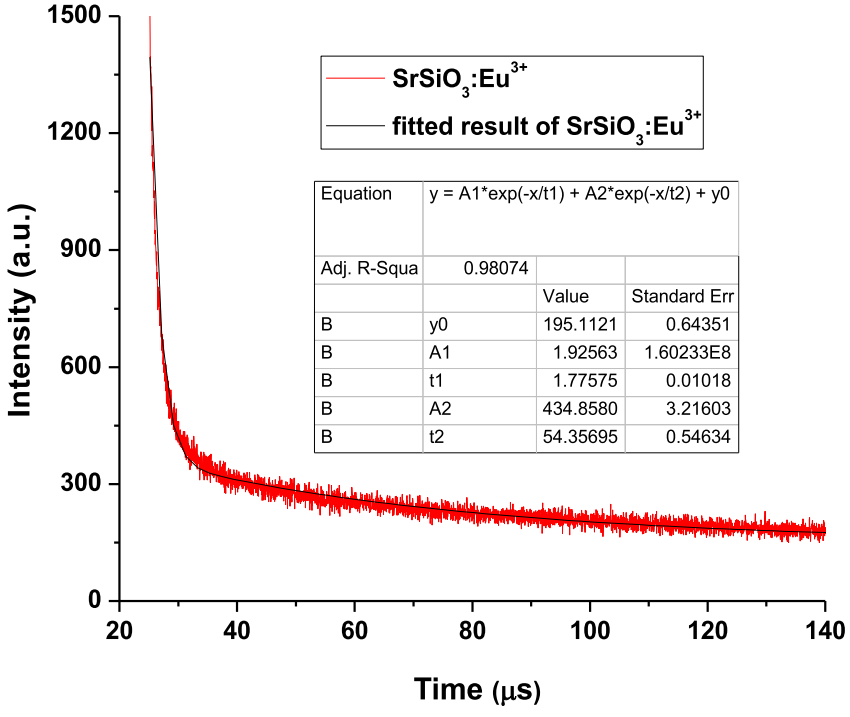

Fig. 7. Decay curves of $SrSiO_3:Eu^{3+}$ phosphor.

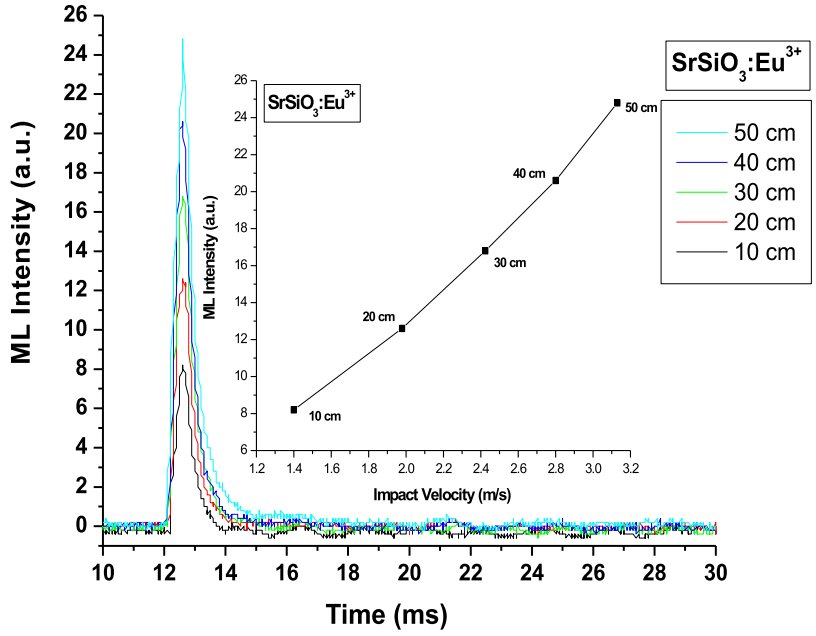

Fig. 8. ML intensity versus time curve of $SrSiO_3:Eu^{3+}$ phosphor (Inset – ML intensity versus impact velocity curve of $SrSiO_3:Eu^{3+}$ phosphor.

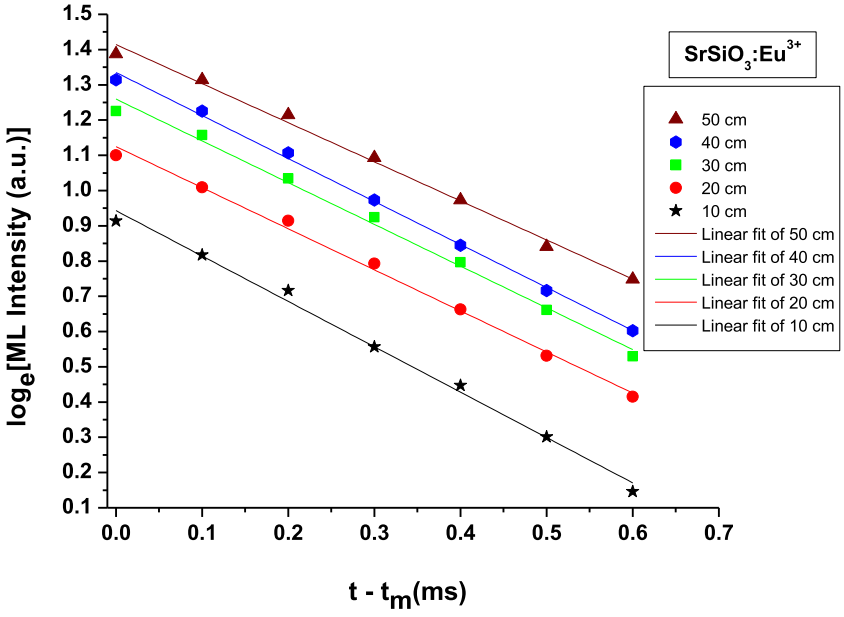

Fig. 9. Semi-log plot of ML intensity versus ($t-t_m$) for $SrSiO_3:Eu^{3+}$ phosphor.

Table 3
Calculation of ML decay constant.

Impact velocity	10 cm	20 cm	30 cm	40 cm	50 cm
τ Decay constant (ms)	0.77	0.85	0.84	0.82	0.90
Standard error (ms)	0.01	0.01	0.02	0.01	0.02

ML excitation may be caused by the local piezoelectric field near the impurities and defects that are in the phosphor. During the impact on the material, one of its newly created surfaces gets positively charged and the other surface crack gets negatively charged (Fig. 11). Thus, an intense electric field in the order of 10^6–10^7 V/cm was produced [50]. Under such order of electric field, the ejected electrons from the negatively charged surface may be accelerated and subsequently their impact on the positively charged surfaces may excite the luminescence center. At the height of the moving piston increases; the area of newly created surface increases, hence free electrons and holes were generated and the subsequent recombination of electrons/hole with the electron/hole trap centers gave rise to light emission.

The impact velocity will be equal to the impact pressure (P_0) i.e., $P_0 = Z\upsilon_0$, where Z is a constant. With the increasing value of impact velocity, the trap depth will decrease, therefore, the trap depth beyond a particular pressure the traps will be unstable and they will be de-trapped, in which the number of de-trapped electrons

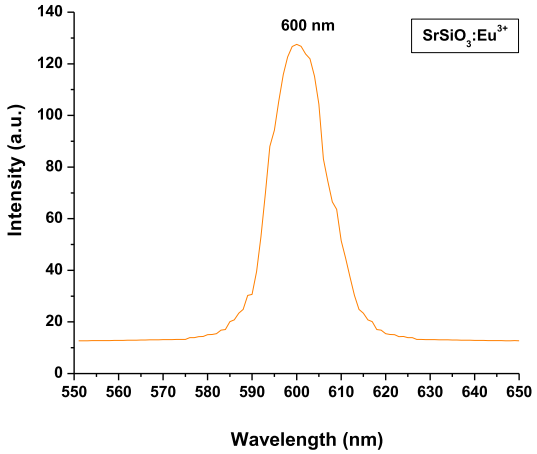

Fig. 10. ML spectrum of $SrSiO_3:Eu^{3+}$ phosphor.

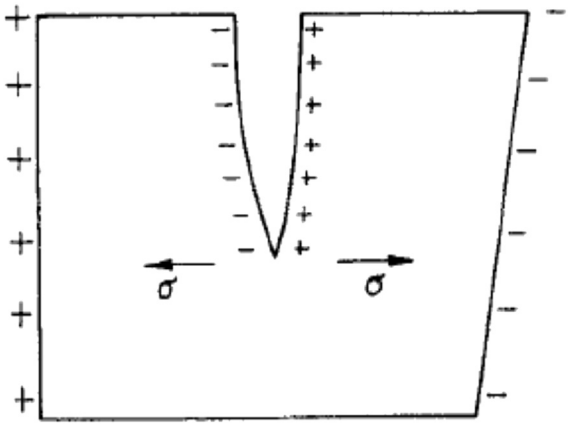

Fig. 11. Langevin model for the piezo-electrification induce phosphor.

will increase with the increasing impact velocity. Thus, the ML intensity will increase proportionally with increasing value of impact velocity [51]. As the impact velocity increases, the impact pressure also increases, leading to increase in the electric field at local region which causes decrease in trap depth. Hence the probability of detrapping increases. From Fig. 8 (inset), it can be seen that with increasing impact velocity, ML intensity also increases linearly i.e., the ML intensity of $SrSiO_3:Eu^{3+}$ phosphor is linearly proportional to the magnitude of the impact velocity. When the surface of an object was coated with the ML materials, the stress distribution in the object beneath the layer could be reflected by the ML brightness and could be observed. Based on the above analysis these phosphors can also be used as sensors to detect the stress of an object [52].

4. Conclusion

An orange–red emitting $SrSiO_3:Eu^{3+}$ phosphor was synthesized by high temperature solid state reaction method at 1250 °C and its structural characterization and luminescence properties were systematically investigated. The monoclinic structure of the prepared phosphor was confirmed by XRD. The PL measurements showed that the phosphor exhibited an emission peak with good intensity at 594 and 614 nm, corresponding to the $^5D_0 \rightarrow {}^7F_1$ orange emission and the weak $^5D_0 \rightarrow {}^7F_2$ red emission. The excitation band at 396 nm can be assigned to $^7F_0 \rightarrow {}^5L_6$ transition of Eu^{3+} ions due to the typical f–f transitions. TL, PL and ML spectra confirm the discussed $SrSiO_3:Eu^{3+}$ phosphor exhibits the orange–red emission and excellent color stability. The chromaticity coordinates (x, y) of this phosphor are calculated to be (x = 0.564, y = 0.415). The color purity of $SrSiO_3:Eu^{3+}$ has been determined to 99.62%, indicating that almost pure orange-red color purity was obtained in this work. Moreover, the quantum efficiency of $SrSiO_3:Eu^{3+}$ phosphor has been obtained, which is higher than the commercial red phosphors. All these characteristics suggest that the orange–red-emitting $SrSiO_3:Eu^{3+}$ phosphor may be a suitable component of phosphor-converted W-LEDs. It is worthy to note that the dependence between the ML intensity of $SrSiO_3:Eu^{3+}$ and the impact velocity of the moving piston is nearly linear, which suggests these phosphors can also be used as sensors to detect the stress of an object.

References

[1] H.W. Leverenz, An Introduction to Luminescence of Solids, Dover Publications Inc., New York, 1968.
[2] N. Lakshminarasimhan, U.V. Varadaraju, Luminescence and afterglow in Sr_2SiO_4: Eu^{2+}, RE^{3+} [RE = Ce, Nd, Sm and Dy] phosphors – role of co-dopants in search for afterglow, Mater. Res. Bull. 43 (2008) 2946–2953.
[3] I.P. Sahu, D.P. Bisen, N. Brahme, Structural characterization and optical properties of $Ca_2MgSi_2O_7:Eu^{2+}$, Dy^{3+} phosphor by solid state reaction method, J. Biol. Chem. Lumin. 30 (5) (2015) 526–532.
[4] F.W. Kang, Y. Hu, L. Chen, X.J. Wang, H. Wu, Z. Mu, Luminescent properties of Eu^{3+} in MWO_4 (M=Ca, Sr, Ba) matrix, J. Lumin. 135 (2013) 113–119.
[5] Z. Song, J. Liao, X. Ding, T. Zhou, Q.L. Liu, Stability of divalent/trivalent oxidation state of europium in some Sr-based inorganic compounds, J. Lumin. 132 (2012) 1768–1773.
[6] T.W. Kuo, T.M. Chen, Synthesis and luminescence of $Ca_4YO(BO_3)_3:Eu^{3+}$ for fluorescent lamp application, Opt. Mater. 32 (2010) 882–885.
[7] H. Wu, Y. Hu, G. Ju, L. Chen, X. Wang, Z. Yang, Photoluminescence and thermoluminescence of Ce^{3+} and Eu^{2+} in $Ca_2Al_2SiO_7$ matrix, J. Lumin. 131 (2011) 2441–2445.
[8] H. Wu, Y. Hu, L. Chen, X. Wang, Investigation on the enhancement and the suppression of persistent luminescence of Re^{3+} doped $Sr_2EuMgSi_2O_7$ (Re = Dy, Yb), J. Alloys Compd. 509 (2011) 4304–4307.
[9] I.P. Sahu, D.P. Bisen, N. Brahme, Luminescence properties of Eu^{2+} and Dy^{3+} doped $Sr_2MgSi_2O_7$ and $Ca_2MgSi_2O_7$ phosphors by solid state reaction method, Res. Chem. Intermed. 41 (9) (2015) 6649–6664.
[10] S. Kamei, Y. Kojima, N. Nishimiya, Preparation and fluorescence properties of novel red-emitting Eu^{3+}-activated amorphous alkaline earth silicate, J. Lumin. 130 (2010) 2247–2250.
[11] I.P. Sahu, D.P. Bisen, N. Brahme, L. Wanjari, R.K. Tamrakar, Structural characterization and luminescence properties of bluish-green emitting $SrCaMgSi_2O_7:Eu^{2+}$, Dy^{3+} phosphor by solid state reaction method, Res. Chem. Intermed. 41 (11) (2015) 8797–8814.
[12] Y. Xu, D. Chen, Combustion synthesis and photoluminescence of $Sr_2MgSi_2O_7$: Eu, Dy long lasting phosphor nanoparticles, Ceram. Int. 34 (2008) 2117–2127.
[13] M. Xu, L. Wang, L. Liu, D. Jia, R. Sheng, Influence of Gd^{3+} doping on the luminescent of $Sr_2P_2O_7:Eu^{3+}$ orange-red phosphors, J. Lumin. 146 (2014) 475–479.
[14] I.P. Sahu, The role of europium and dysprosium in the bluish-green long lasting $Sr_2Al_2SiO_7:Eu^{2+}$, Dy^{3+} phosphor by solid state reaction method, J. Mater. Sci. Mater. Electron. 26 (9) (2015) 7059–7072.
[15] JCPDS file number 24-1230, JCPDS International Center for Diffraction Data.
[16] I.P. Sahu, D.P. Bisen, R.K. Tamrakar, R. Shrivastava, Enhancement of the photoluminescence and long afterglow properties of $Ca_2MgSi_2O_7:Eu^{2+}$ phosphor by Dy^{3+} co-doping, Res. Chem. Intermed. 42 (2016) 1823–1843.
[17] I.P. Sahu, D.P. Bisen, N. Brahme, R.K. Tamrakar, Luminescence enhancement of bluish – green $Sr_2Al_2SiO_7:Eu^{2+}$ phosphor by dysprosium co-doping, J. Lumin. 167 (2015) 278–288.
[18] I.P. Sahu, D.P. Bisen, N. Brahme, Dysprosium doped di-strontium magnesium di-silicate white light emitting phosphor by solid state reaction method, Displays 35 (5) (2014) 279–286.
[19] M.A. Salim, R. Hussain, M.S. Abdullah, S. Abdullah, N.S. Alias, The local structure of phosphor material, $Sr_2MgSi_2O_7$ and $Sr_2MgSi_2O_7:Eu^{2+}$ by infrared spectroscopy, Solid State Sci. Technol. 17 (2009) 59–64.
[20] Z. Gou, J. Chang, W. Zhai, Physical properties of 8 mol% Ceria doped yttria stabilised zirconia powder and ceramic and their behaviour during annealing and sintering, J. Eur. Ceram. Soc. 25 (2005) 1507–1514.
[21] I.P. Sahu, D.P. Bisen, N. Brahme, Structural characterization and optical properties of dysprosium doped strontium calcium magnesium di-silicate phosphor by solid state reaction method, Displays 38 (2015) 68–76.
[22] G.T. Chandrappa, S. Ghosh, K.C. Patil, Synthesis and properties of willemite, Zn_2SiO_4, and $M^{2+}:Zn_2SiO_4$ (M = Co and Ni), J. Mater. Syn. Process. 7 (1999) 273–279.
[23] Z. Yuan, C. Chang, D. Mao, W.J. Ying, Effect of composition on the luminescent properties of $Sr_4Al_{14}O_{25}$: Eu^{2+}, Dy^{3+} phosphors, J. Alloys Compd. 377 (1–2) (2004) 268–271.

[24] I.P. Sahu, D.P. Bisen, N. Brahme, R.K. Tamrakar, Enhanced luminescence performance of $Sr_2MgSi_2O_7:Eu^{2+}$ blue long persistence phosphor by co-doping with Ce^{3+} ions, J. Mater. Sci. Mater. Electron. 27 (1) (2015) 554–569.
[25] T. Katsumata, R. Sakai, S. Komuro, T. Morikawa, Thermally stimulated and photostimulated luminescence from long duration phosphorescent $SrAl_2O_4$: Eu, Dy crystals, J. Electrochem. Soc. 150 (2003) 111–114.
[26] I.P. Sahu, D.P. Bisen, N. Brahme, M. Ganjir, Enhancement of the photoluminescence and long after glow properties of $Sr_2MgSi_2O_7:Eu^{2+}$ phosphor by Dy^{3+} co-doping, Lumin. J. Biol. Chem. Lumin. 30 (8) (2015) 1318–1325.
[27] V. Pagonis, G. Kitis, C. Furetta, Numerical and Practical Exercises in Thermoluminescence, Springer, 2006.
[28] R. Chen, S.W.S. McKeever, Theory of Thermoluminescence and Related Phenomenon, World Scientific Press, Singapore, 1997.
[29] C. Devayani, S.K. Omanwar, S.V. Moharil, Luminescence properties of red emitting phosphor $NaSrBO_3:Eu^{3+}$ prepared with novel combustion synthesis method, J. Lumin. 142 (2013) 180–183.
[30] G. Vicentinia, L.B. Zinner, J. Zukerman-Schpector, K. Zinner, Luminescence and structure of europium compounds, Coord. Chem. Rev. 196 (2000) 353–382.
[31] H.Y. Jiao, Y. Wang, A potential red-emitting phosphor $CaSrAl_2SiO_7:Eu^{3+}$ for near-ultraviolet light-emitting diodes, Phys. B 407 (2012) 2729–2733.
[32] H. Nagabhushana, D.V. Sunitha, S.C. Sharma, B. Daruka Prasad, B.M. Nagabhushana, R.P.S. Chakradhar, Enhanced luminescence by monovalent alkali metal ions in $Sr_2SiO_4:Eu^{3+}$ nanophosphor prepared by low temperature solution combustion method, J. Alloys Compd. 595 (2014) 192–199.
[33] CIE (1931) International Commission on Illumination. Publication CIE no. 15 (E-1.3.1).
[34] Z. Lou, J. Hao, Cathodoluminescence of rare-earth-doped zinc aluminate films, Thin Solid Films 450 (2004) 334–340.
[35] J. Suresh Kumar, K. Pavani, A. Mohan Babu, N. Kumar Giri, S.B. Rai, L.R. Moorthy, Fluorescence characteristics of Dy^{3+} ions in calcium fluoroborate glasses, J. Lumin. 130 (2010) 1916–1923.
[36] T. Aitasalo, J. Holsa, H. Jungner, M. Lastusaari, J. Niittykoski, Thermoluminescence study of persistent luminescence Materials: Eu^{2+}- and R^{3+}-doped calcium aluminates, $CaAl_2O_4:Eu^{2+}$, R^{3+}, J. Phys. Chem. B 110 (2006) 4589–4598.
[37] X.M. Han, J. Lin, M. Yu, C.K. Lin, X.W. Qi, Z.Y. Yu, X.Q. Wang, Luminescence properties of spherical phosphors $SrSiO_3:Eu^{3+}$, Key Eng. Mater. 336–338 (2007) 619–621.
[38] S. Long, J. Hou, G. Zhang, F. Huang, Y. Zeng, High quantum efficiency red-emission tungstate based phosphor $Sr(La_{1-x}Eu_x)_2Mg_2W_2O_{12}$ for WLEDs application, Ceram. Int. 39 (2013) 6013–6017.
[39] R. Yu, C. Wang, J. Chen, Y. Wu, H. Li, H. Ma, Oxy-fluoride phosphors for solid state lighting, ECS J. Solid State Sci. 3 (2014) 33–37.
[40] Y.Q. Li, J.E.J. van Steen, J.W.H. van Krevel, G. Botty, A.C.A. Delsing, F.J. DiSalvo, G. de, H.T.J.M. Hintzen, Luminescence properties of red-emitting $M_2Si_5N_8:Eu^{2+}$ (M = Ca, Sr, Ba) LED conversion phosphors, J. Alloys Compd. 417 (2006) 273–279.
[41] J. Hou, X. Yin, Y. Fang, F. Huang, W. Jiang, Novel red-emitting perovskite-type phosphor $CaLa_{1-x}MgM'O_6$: xEu^{3+} (M′ = Nb, Ta) for white LED application, Opt. Mater. 34 (2012) 1394–1397.
[42] D.R. Vij, Luminescence of Solids, Plenum Press, New York, 1998.
[43] B.P. Chandra, Development of mechanoluminescence technique for impact studies, J. Lumin. 131 (2011) 1203–1210.
[44] I.P. Sahu, D.P. Bisen, N. Brahme, R.K. Tamrakar, Studies on the luminescence properties of europium doped strontium alumino-silicate phosphors by solid state reaction method, J. Mater. Sci. Mater. Electron. 26 (2015) 10075–10086.
[45] I.P. Sahu, D.P. Bisen, N. Brahme, Luminescent properties of green emitting $Ca_2MgSi_2O_7:Eu^{2+}$ phosphor by solid state reaction method, Lumin. J. Biol. Chem. Lumin. 30 (7) (2015) 1125–1132.
[46] I.P. Sahu, P. Chandrakar, R.N. Baghel, D.P. Bisen, N. Brahme, R.K. Tamrakar, Luminescence properties of dysprosium doped calcium magnesium silicate phosphor by solid state reaction method, J. Alloys Compd. 649 (2015) 1329–1338.
[47] H. Zhang, N. Terasaki, H. Yamada, C.N. Xu, Development of mechanoluminescent micro-particles $Ca_2MgSi_2O_7:Eu$, Dy and their application in sensors, Thin Solid Films 518 (2009) 610–613.
[48] I.P. Sahu, D.P. Bisen, R.K. Tamrakar, R.K. Tamrakar, R. Shrivastava, Dysprosium doped di-calcium magnesium di-silicatewhite light emitting phosphor by solid state reaction method, J. Mater. Sci. Mater. Electron. 26 (2015) 9907–9920.
[49] I.P. Sahu, D.P. Bisen, N. Brahme, Europium doped di-calcium magnesium di-silicate orange-red emitting phosphor by solid state reaction method, J. Radiat. Res. Appl. Sci. 8 (2015) 381–388.
[50] I.P. Sahu, D.P. Bisen, N. Brahme, R.K. Tamrakar, Photoluminescence properties of europium doped di-strontium magnesium di-silicate phosphor by solid state reaction method, J. Radiat. Res. Appl. Sci. 8 (2015) 104–109.
[51] H. Zhang, N. Terasaki, H. Yamada, C.N. Xu, Blue light emission from stress activated $Sr_2MgSi_2O_7$:Eu, Int. J. Mod. Phys. B 23 (2009) 1028–1033.
[52] H. Zhang, C.N. Xu, N. Terasaki, H. Yamada, Detection of stress distribution using $Ca_2MgSi_2O_7$:Eu,Dy microparticles, Phys. E 42 (2010) 2872–2875.